Leveraging Single Protein Polymers To Measure Flexural Rigidity†

Joost van Mameren,[†,||] Karen C. Vermeulen,[†] Fred Gittes,[‡] and Christoph F. Schmidt*[,†,§]

Laser Centre and Department of Physics and Astronomy, Vrije Universiteit, De Boelelaan 1081, 1081 HV Amsterdam, The Netherlands, Department of Physics, Washington State University, Webster Building, Pullman, Washington 99164-2814, and 3. Physikalisches Institut, Fakultät für Physik, Georg-August-Universität, Friedrich-Hund-Platz 1, 37077 Göttingen, Germany

Received: September 19, 2008; Revised Manuscript Received: January 27, 2009

The micrometer-scale length of some protein polymers allows them to be mechanically manipulated in single-molecule experiments. This provides a direct way to measure persistence length. We have used a double optical trap to elastically deform single microtubules and actin filaments. Axial extensional force was exerted on beads attached laterally to the filaments. Because the attachments are off the line of force, pulling the beads apart couples to local bending of the filament. We present a simple mechanical model for the resulting highly nonlinear elastic response of the dumbbell construct. The flexural rigidities of the microfilaments that were found by fitting the model to the experimentally observed force−distance curves are $(7.1 \pm 0.8) \times 10^4$ pN·nm^2 (persistence length $L_p = 17.2$ μm) for F-actin and $(6.1 \pm 1.3) \times 10^6$ pN·nm^2 ($L_p = 1.4$ mm) for microtubules.

Introduction

Soft matter owes its typically complex behavior to the multitude of characteristic length and time scales needed to describe it. Scaling approaches introduced in seminal work by Pierre-Gilles de Gennes[1] have been very successful in particular in describing both structure and dynamics of polymer melts and solutions. It was Pierre-Gilles de Gennes who noted the possibility to apply the theory of critical phenomena, developed to describe second order phase transitions, to polymers.[2] Power-law scaling has subsequently been found in many polymer systems.[1] The dynamics of polymer networks can be described by a number of characteristic length scales, such as monomer size, persistence length, mesh size, or molecular contour length. In technical polymers these length scales are often in the angstrom to nanometer regime. Many biopolymers such as DNA or protein polymers exhibit an intriguing spectrum of behavior because here length scales can reach into the micrometer or millimeter regime. This makes it also possible to do experiments on individual polymer strands. Here we focus on single-molecule mechanical experiments with microtubules and actin filaments (F-actin) to determine a crucial characteristic length, namely their persistence length. The persistence length L_p is the exponential decay constant of the thermal tangent-tangent correlation function along the chain, modeled as a homogeneous bendable filament,[3,4] and depends on the flexural rigidity EI of the filament and the temperature T as $L_p = EI/kT$, where k is the Boltzmann constant. Microtubules and actin filaments are protein polymers that are the main constituents of the cytoskeleton of eukaryotic cells. Their limited bending flexibility is of key importance for their range of physiological functions. Both microtubules and actin filaments, for instance, act as tracks for directed movement by motor proteins such as the widely studied dyneins, kinesins, or myosins.[5] Moreover, microtubules are crucial for cell division, where the mitotic spindle, constructed mainly from microtubules, regulates the separation of cellular components into the daughter cells.[5]

Solutions of F-actin have been studied by microrheology, and scaling behavior of the shear elastic moduli has been found[6−9] that can be well explained by models using thermally undulating entangled or cross-linked semiflexible chains,[10,11] using persistence length as a parameter. However, such bulk experiments do not provide a good measure for the single molecule persistence length. Several single-molecule measurements of the flexural rigidity (EI) of actin filaments and microtubules have been reported. Various experimental techniques have been employed in these studies, among which two main classes of experiments can be discerned. In active experiments, the microtubules or actin filaments are actively bent by external forces (e.g., using optical tweezers or viscous flow) and the reacting force is detected.[12−18] In passive or thermal experiments, the motion of the filaments due to the thermal bombardment by surrounding solvent molecules is analyzed.[19,20,12,21−24] Notably, no quantitative agreement has been reached within an order of magnitude for microtubules, and also for actin filaments the spread in previously found values for the flexural rigidity is large. Recently, a model has been proposed that introduces yet another length scale on the order of micrometers for microtubule dynamics that should be relevant if the shear elastic modulus between the 13 so-called protofilaments that make up the hollow microtubules by lateral attachments was extremely low compared to the bulk response of the protofilaments themselves.[25] However, direct measurement of the shear elastic modulus of microtubules has not supported this case.[26−28]

Here, we report a new approach to obtain the flexural rigidity by means of well-controlled active experiments using optical tweezers to bend the filaments locally, as schematically depicted in Figure 1. In this way force-extension curves were measured for taxol-stabilized microtubules and rhodamine-phalloidin-labeled actin filaments. Because of the off-center attachments,

† Part of the "PGG (Pierre-Gilles de Gennes) Memorial Issue".

* To whom correspondence should be addressed. E-mail: cfs@physik3.gwdg.de. Phone: +49 551 397740. Fax: +49 551 397720.

† Vrije Universiteit.

‡ Washington State University.

§ Georg-August-Universität.

|| Current address: JPK Instruments AG, Bouchéstrasse 12, 12435 Berlin, Germany.

10.1021/jp808328a CCC: $40.75
Published on Web 02/16/2009

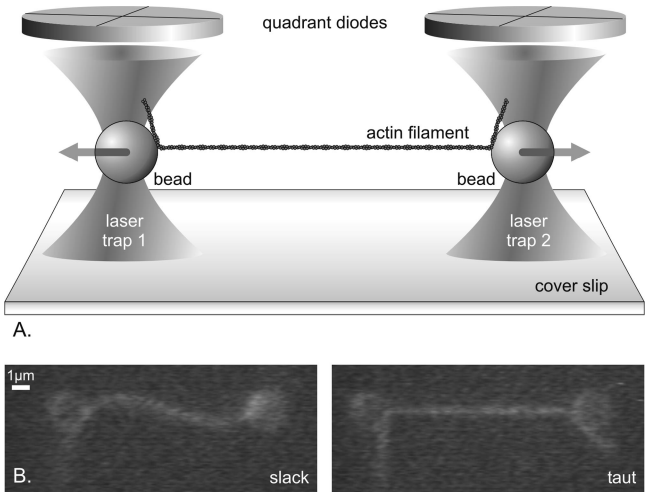

Figure 1. (A) Schematic of the assay used for the bending experiments. Two beads are held by two optical traps, suspending a microtubule or actin filament. The beads are attached laterally to the filaments. Therefore, both torque and outward tension are exerted on the filament when the distance between the traps is increased. Filaments tend to bend in response. (B) Fluorescence microscope images of a slack and taut actin filament, the latter exhibiting a sharp bend near the attachment point to the beads. The distance between the beads was measured from video images. The restoring force of the filament was measured using back-focal plane interferometry.[32,47]

a linear force pulling the beads apart couples to local bending of the filament. The flexural rigidity was determined from a fit of a mechanical model to the data, modeling the filaments as homogeneous elastic rods. A numerical solution to this model is presented since the differential equations cannot be integrated analytically. We also derived approximate analytical expressions for three asymptotic regimes.

This experiment provides a very sensitive measure of bending rigidity and, in principle, allows one to explore length dependent response as well as effects of defects and structural inhomogeneities. A further motivation for the study was that the geometry studied here is frequently used in single molecule assays for nonprocessive motor proteins, in so-called three-bead assays. In such assays, filaments, F-actin or microtubles are suspended by two optically trapped bead above a motor protein, attached to a third bead fixed on the substrate surface, which exerts force on the suspended filaments.[29,15,30,31] The lateral attachment of beads to the protein filament introduces additional compliance that can strongly affect the time resolution of the experiment. Using mechanical parameters for F-actin and microtubules, our model predicts, counterintuitively, that at low tension, the effective compliance of a microtubule construct can be less than that of an actin construct, although actin filaments are about 100× less rigid than microtubules.

For laterally attached beads, the softest component in this attachment is generated by the bending of the filaments due to the torque exerted by the laterally attached beads (Figure 1). Even for the relatively rigid microtubules this compliance is rather large unless pretension is applied between the two beads. With increasing pretension, the connection stiffens in a highly nonlinear fashion. This problem has been treated approximatively earlier.[15,30] The stiffness of the bead-filament-bead construct can be calculated more precisely using the values for the flexural rigidity obtained through the experiments and the numerical solution to the model presented in this study.

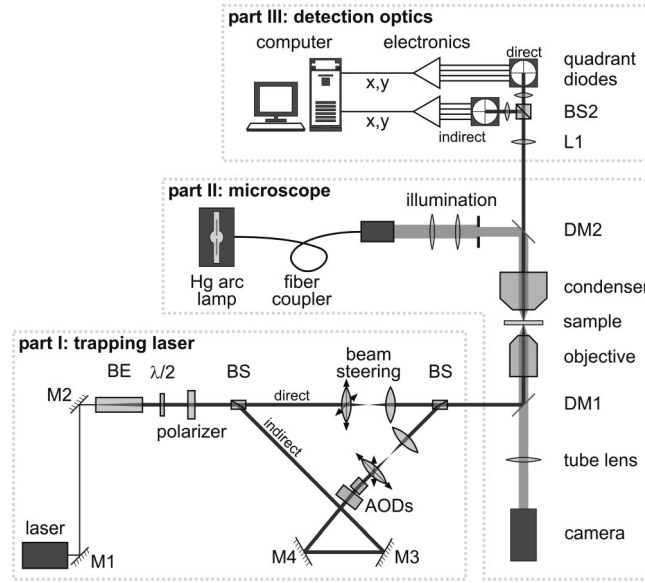

Figure 2. Diagram of the experimental setup. The laser is expanded (BE), attenuated by a $\lambda/2$ plate and a polarizer, and split in two orthogonally polarized beams by a polarizing beam splitter (BS). One beam is continuing straight through a pair of telescope lenses that serve for beam steering, the other is directed through a pair of AODs and then through telescope lenses. Beams are joined by BS2 and coupled into the microscope via a dichroic DM1 and, after passing objective, sample, and condenser, guided to the detectors via polarizing beam splitter BS2.

Materials and Methods

Optical Tweezers Setup. The setup used for optical trapping is schematically represented in Figure 2 and was described in detail earlier[32−35] apart from a few adaptations. A set of Glan-Laser polarizing beam splitters was introduced to create a second optical trap. In one of the light paths, two orthogonally oriented acousto-optic deflectors (model DTD-276HB6, IntraAction Corp., Bellwood, IL) were placed for additional computer-controlled high-resolution positioning of one of the traps. The RF signals for the acousto-optic deflectors (AODs) (18 MHz bandwidth, 26 MHz center frequency) are synthesized by a two-channel 16-bit PCI-board. Tight room temperature control (within 1 °C) in the laboratory largely reduced beam-pointing instabilities. The two (x, y) displacement signals are sampled by a data acquisition board (16-bit, σ-δ, AD16/ChicoPlus, Innovative Integration, Simi Valley, CA). The $\Sigma\Delta$ conversion makes the use of antialias filters[32,36,37] superfluous. The data is further processed with custom-written software (LabVIEW, National Instruments, Austin, TX). The microscope can be used both in transillumination DIC mode for microtubules and in epifluorescence mode for rhodamine-phalloidin-labeled actin filaments. The sample was imaged onto a camera (model VT1000 for DIC, model VT1000 SIT for fluorescence, Dage-MTI, Michigan City, IN) and digitally analyzed using a PCI-1407 image acquisition board and the Vision software package for LabVIEW (both National Instruments, Austin, TX).

Filament Preparation. Tubulin was purified from pig brain by two cycles of assembly and disassembly followed by chromatography on phosphocellulose following a standard recipe[38] and stored at −80 °C. The tubulin was biotinylated in a 1:20 molar ratio by adding commercial biotinylated tubulin (T333-B, Cytoskeleton, Denver, CO) and supplemented with 10% glycerol and 1 mM GTP. The protein mixture was stored in 2 μL aliquots at −80 °C. To prepare samples, tubulin was thawed and incubated for 30 min at 35 °C. Subsequently, the

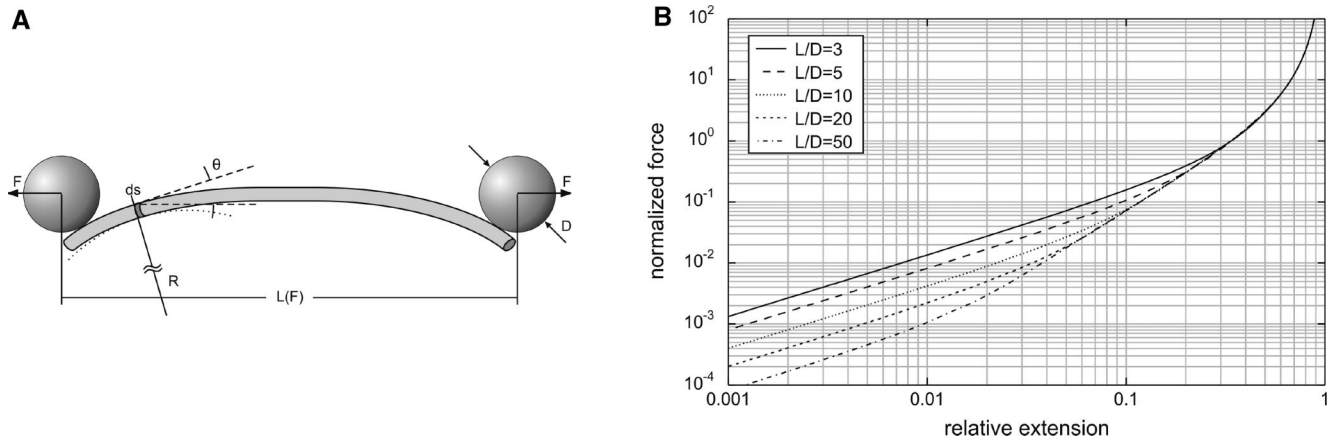

Figure 3. (A) Mechanical model for the lateral attachment of a filament to two beads of diameter *D* separated by a length *L* measured along the filament and pulled apart by a force *F*. A few more geometrical parameters are introduced graphically. The local radius of curvature of the filament is here designated by *R*. The numerically calculated predictions for force as a function of extension, obtained as explained in Supporting Information, are shown in panel (B) for different values of the ratio *L*/*D*.

microtubules were diluted 200−500 times in PEM80 buffer (80 mM Pipes pH 6.9, 1 mM EGTA, 2 mM MgCl2) including 10 μM taxol. Microtubules were kept at room temperature and protected from light for use for at most one day.

Actin was purified from acetone powder obtained from rabbit skeletal muscle following established recipes[39] and biotinylated by adding biocytin maleimide (Molecular Probes) dissolved in DMSO (6.6 mM)[40] to an approximate biotinylation ratio (biotin-actin/unlabeled actin) of 1:1−4. Aliquots of 2 μL were stored in unpolymerized form at −80 °C in G-buffer (pH 7.5, 2 mM Tris-Cl, 0.2 mM CaCl2, 0.5 mM DTT, 0.2 mM ATP).

Actin was polymerized by thawing an aliquot and incubating at room temperature for 30 min in F-buffer (pH 7.5, 2 mM HEPES, 2 mM MgCl2, 50 mM KCl, 1 mM Na2ATP, 1 mM EGTA). Actin filaments were subsequently diluted 100−200 times by adding 10× concentrated F-buffer, degassed, double-distilled H_2O supplemented with antibleach buffer (10 mM glucose, 10 mM glucose oxidase, 10 mM catalase, 10 mM DTT).[41] Filaments were fluorescently labeled with TRITC-phalloidin (Sigma) to achieve a ratio of about one phalloidin per actin monomer. F-actin was kept on ice for use for at most one day.

Both, actin filaments and microtubules were specifically attached to beads coated with avidin/streptavidin linkers (2.17 μm diameter, streptavidin on polystyrene, Spherotech, Libertyville, IL; or 1.5 μm diameter, avidin on silica, Bangs Laboratories, Fishers, IN). Beads were washed twice and resuspended in a buffer appropriate for the type of filaments used (PEM80 for microtubules, F-buffer for actin filaments).

Bending Experiments. Sample chambers were constructed from a coverslip attached with two narrow strips of double stick tape to a microscope slide. Chambers were filled with biotinylated filaments diluted another ten times in their appropriate buffers to a volume of ~15 μL and supplemented with streptavidin-coated beads in such a concentration that about one bead appeared per two microscope fields of view (~30 μm).

A bead was trapped in each laser trap, approximately 10 μm above the substrate surface to avoid hydrodynamic surface effects. Position data for the beads, measured by the two quadrant diodes, was recorded at 20 kHz for about fifteen seconds and used for off-line trap calibration using power spectral density analysis.[42,43,37,36,44,45]

By moving the microscope stage, a filament was brought into the vicinity of one of the two beads and attached to it. Next, the free end was attached to the other bead by flow induced by moving the stage. Typically the bead−bead distance was on the order of micrometers with the microtubules or actin filaments not much longer than that. After establishing the bead-filament-bead constructs, they were subjected to periodic stretching and relaxing, accomplished by longitudinally displacing the AOD-steered trap in a triangular or sinusoidal fashion. The amplitude of the oscillations controlled the maximum pulling force on the constructs. Trap oscillation frequencies were sufficiently low (typically 0.1 Hz) to avoid additional force due to viscous drag on the bead or the filament.

Microscope images (at standard 25 Hz video rate) and quadrant-diode displacement signals from the beads in their traps (2 kHz) were recorded for offline analysis of force and distance. The digitized video recordings were analyzed using LabVIEW software to obtain the interbead distance as a function of time, which was then synchronized with the force data. Next, the distance data were spline-interpolated in order to allow us to plot high-resolution force data versus distance data in a scatter plot, eliminating time.

Theoretical Model

In order to interpret the experimentally observed force-extension curves, we developed a model that describes the microtubules and actin filaments as thin, inextensible elastic rods with arbitrary cross-section (this includes solid rods and hollow tubes) whose bending properties can be described by a flexural rigidity *EI*.[46] The geometrical factor *I* describes the cross section of the rods. These rods are bent by two opposed torque forces acting at a distance equal to the bead radius as shown in Figure 3A. This system is governed by the so-called beam equation[46]

$$M(s) = EI\frac{\mathrm{d}\theta(s)}{\mathrm{d}s} \tag{1}$$

where *M* is the bending moment at point *s* along the filament, *EI* is the flexural rigidity of the filament, and $\mathrm{d}\theta(s)/\mathrm{d}s$ is the local curvature induced by *M*. Taking into account that external forces are applied at isolated points only, eq 1 can be integrated once to yield

$$\frac{d\theta}{ds} = \sqrt{\frac{F}{EI}(C - 2\cos\theta)} \quad (2)$$

with C a constant, as shown in Supporting Information. This equation can be solved numerically to obtain model force-extension curves, shown in Figure 3B for different filament length and bead diameter ratios (L/D). The figure shows dimensionless forces, obtained by multiplying with D^2/EI. The relative extension, designated by X, is measured as the extension $\xi = L(F) - L$, that is, the difference between the distance of the two beads at a certain force, $L(F)$, and the relaxed length, $L(0) \equiv L$, scaled by the bead diameter D (therefore $0 \leq X = \xi/D \leq 1$). The force-extension curves can be piecewise approximated in three force regimes, indicated in Figure 4A and described in more detail in Supporting Information. For a weak force, the filament will be slightly curved along its entire length, which gives a linear force-extension relationship. At intermediate forces, the center part of the filament will approach the line of force between the two bead centers and become straight. In this regime the force-extension relation is approximately quadratic. For high forces, the curvature will become strongly localized near the attachment points of the beads with the bend in the filament approaching 90°. In this regime, the response becomes highly nonlinear. For $L/D = 50$, the approximations are shown in Figure 4B as dark gray lines. Between the ranges of validity of the intermediate and high force approximations, the following interpolating formula matches the numerical results nicely:

$$F = \frac{EI}{D^2}\left(\frac{8}{3}X + 2(2 - \sqrt{2})\frac{X^2\sqrt{X}}{1 - X}\right)^2 \quad (3)$$

As discussed in the Supporting Information, this formula gives as limits the two physically derived equations (S7 and S8) as follows. For small X, it predicts $F = (EI/D^2)(64/9)X^2$, correctly describing forces in the intermediate regime, where the force is quadratic in the extension. As X approaches 1, it predicts $F = (EI/D^2)8(3-2(2)^{1/2}/(1-X)^2)$, which correctly describes the force dependence in the high-force regime, where the force on the (assumed inextensible) polymer becomes very large with increasing extension. It is evident from a comparison of Figure 4 and Figure 5 that only these two regimes, and not the low-force regime, are relevant to our measurements. It can be seen from Figure 4B and the approximating equations in the Supporting Information that only the low-force regime depends on the ratio L/D. The crossover point between low and intermediate force regime shifts to higher forces for a lower ratio L/D. Even for short filaments (with low L/D), the best signal-to-noise ratio was obtained in the higher-force regimes. Therefore, the departure of the interpolating formula (eq 3) from the numerical results at low forces can be safely ignored when eq 3 is used to fit the model to the data and a value for EI is extracted for each construct.

Results

Model Fitting. The force−distance curve that was acquired for each bead-filament-bead construct was fit by the model (eq 3) in the following manner. First, independently determined parameters were fixed: the bead diameter (supplied by the manufacturer within 5%) and an upper limit in the force data to eliminate data outside the linear regime of the optical trap.[32,47]

The relaxed construct length L is experimentally difficult to determine due to the fact that the filaments were thermally fluctuating at zero tension. Therefore, L was treated in the nonlinear fitting routine as a fit parameter.

All constructs eventually broke above a certain force (anywhere between 2−10 pN). Since these forces were well below the typical biotin−streptavidin bond strength (>90 pN),[48] it is most likely that these breakage events were caused by filament imperfections, which might be induced either by photodamage due to the trapping laser light or by the fact that filament curvature and tension become strongly localized at higher forces. As a consequence of these breakage events, the force-extension curves for microtubules went up to a lower maximum relative extension X than those for actin filaments, since microtubules are much stiffer.

Actin Results. Figure 5A shows the force-extension curves measured for Actin filaments. Data was recorded for seven actin constructs (all with bead diameter $D = 2.2$ μm). The data were piecewise averaged to reduce the intrinsic noise in the force signal due to Brownian motion of the beads. By applying an oscillatory extensional force on the beads, the reproducibility of the measurements could be monitored and potential variations over time could be detected. Several constructs were analyzed two or three times in a row in order to control for chemical or mechanical degradation over time. Some constructs were also separately analyzed in the stretching and relaxing directions to look for hysteresis. Neither degradation effects nor hysteresis effects were observed: individual data sets taken with the same construct were consistent. By fitting eq 3 to the data shown in Figure 5A, a value of the flexural rigidity EI was obtained for each construct. This value and the bead diameter were used to calculate the normalized, dimensionless forces (normalized force $= FD^2/EI$) shown in Figure 6A. The collapse of all results on a master curve indicates that the individual curves were well described by the model. The average value found for the flexural rigidity of actin is $EI = (7.1 \pm 0.8) \times 10^{-26}$ nm^2 (standard error of the mean). This corresponds to a persistence length L_p for actin of 17 ± 2 μm using $L_p = EI/k_BT$.[4]

Microtubule Results. Force-extension curves for microtubules are shown in Figure 5B. Data were recorded for eight different microtubule constructs (four with bead diameter $D = 2.2$ μm, four with $D = 1.5$ μm). The same consistency checks were performed with the microtubule constructs as described for actin, assuring the absence of degradation or hysteresis. The curves in Figure 5B are scaled by D^2 in order to allow comparison of microtubule constructs with different bead diameters (see eq 3). Figure 6B shows the curves after scaling by the individual EI values, indicating good agreement with the model as in the case of actin. Upon averaging, we obtained $EI = (6.1 \pm 1.3) \times 10^{-24}$ nm^2 or, equivalently, $L_p = 1.4 \pm 0.3$ mm. What is conspicuous when one compares the microtubule results with the actin results is the considerable dispersion of the force-extension curves observed in the case of microtubules which gives rise to a variation of fitted EI values over about a decade in total. Possible reasons for this widely varying behavior will be addressed in the discussion.

Discussion

The flexural rigidities of actin and microtubules have been investigated earlier in a variety of active and passive experiments. Tables 1 and 2 list reported values for the flexural rigidity of rhodamine-phalloidin-labeled F-actin and (mainly) taxol-stabilized microtubules, respectively. Corresponding persistence lengths and the values found in this study are listed as well.

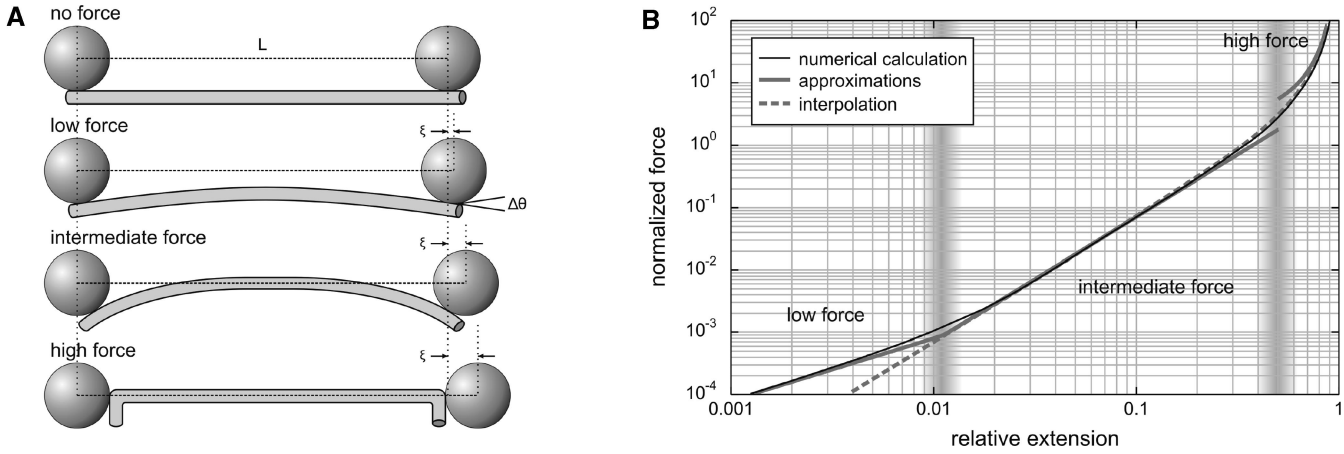

Figure 4. Approximative solutions to the model. The deformations of the bead-filament constructs in the three approximative regimes are qualitatively shown in (A). At low force, the weak curvature extends over the full filament. At intermediate forces, the curvature becomes localized as the middle part of the filament approaches the line of force between the beads. At high forces, the curvature becomes localized at the attachment points to the beads, and the bend angle at these points approaches 90°. The approximative solutions and the according interpolating formula, used for fitting of the data, are plotted in panel (B).

There are a few general differences between active and passive (thermal) experiments. In the case of thermal experiments, one analyzes the amplitudes of thermally excited bending modes from video recordings. Typically, only a few of the longest modes can be considered due to the rapidly decreasing amplitudes with mode number, causing rapidly decreasing signal-to-noise ratios.[49] By definition, one probes the linear response regime when analyzing thermal fluctuations. In contrast, in active experiments much higher forces are typically applied to the filaments, usually at isolated points along the contour length. As in the present case, nonlinearities in the mechanical response often cannot be neglected. Moreover, local filament defects are more likely to play a role for active than for thermal experiments due to the localized application of forces.

We have here determined the flexural rigidity of microtubules and F-actin from a fit of force versus extension data with our nonlinear mechanical model. Incorporated in the model are a few basic assumptions. First, the filaments are assumed to be inextensible; any stretching of the monomer spacing due to the applied force is neglected. In reality, actin filaments (of 10 μm length) have a stretching stiffness of about 5 pN/nm,[50,51] and microtubules with twice as much cross-sectional area have a stretching stiffness of approximately 10 pN/nm. Our assumption of inextensibility is justified by the observation that these values are orders of magnitude larger than the typical stiffness of the lateral bead-filament attachments, as is indicated by the horizontal arrow in Figure 7. Second, thermal restoring forces (entropic spring) are neglected. This assumption is valid for forces greater than k_BT/L_p,[52] corresponding to forces in the subfemtonewton range for both actin and microtubules. An important assumption in our present model is that the beads are bound directly to the filaments. In practice, a finite streptavidin linker attaches the beads to the filaments via two biotins, which complicates the analysis by introducing a second contact point between bead and filament, forming a triangle with the linker attachment point and the center of the bead. Instead of initially purely bending the filament, outward forces on the beads tend to axially stretch the filament since the force acting through the linker attachment has a progressively shorter lever arm for increasing forces. While this effect is difficult to quantify, it is reasonable to neglect it because of the small dimensions of the linker compared to the bead diameter. For bulkier linker molecules than streptavidin/biotin, such as NEM-myosin,[15,30] the effect will probably induce qualitatively different force-extension behavior. Finally, our model assumes that the filaments can be described as homogeneous rods without taking into account their microscopic geometry. Studies in which the tip of a scanning force microscope was used to locally indent microtubules has shown this assumption to be valid down to scales of about 100 nm.[26−28]

The *EI* values and persistence lengths reported in the literature for actin filaments do largely agree on values of $EI \approx 7 \times 10^{-26}$ nm and $L_p \approx 17$ μm with some outliers at up to about four times lower values (see Table 1).

The experimental approach described here is most closely related to that of Dupuis et al.[15] They proposed a mechanical model for the same bead-filament-bead configuration, but made the assumption that the filament bend localized at the beads has a circular shape with a tension-dependent radius. The calculation of the full numerical solution of the equations for the filament bending configuration as described here yields a more precise and reliable analysis.

For microtubules, the literature values for the flexural rigidity are less consistent than for F-actin (see Table 2). Even within our own data, we observe considerable dispersion between different microtubules. There are several possible reasons for this behavior. Janson and Dogterom[24] have shown that the polymerization conditions, and in particular the growth velocity, have an effect on the flexural rigidity of microtubules. There may have been some variation in polymerization conditions in our experiments. The mechanism behind this growth-velocity dependence of the flexural rigidity is unclear. A possible reason is the occurrence of line defects in the 2D crystalline microtubule lattice, that is, jumps in the number of protofilaments within individual microtubules.[53,54] This causes the inner and outer diameter and therefore the bending moment of inertia *I* of the microtubule to vary. Particularly, local steps in protofilament number as observed by Chrétien et al.[53] might influence the behavior at higher tensions, when the bend is getting more and more localized. Since the average protofilament number sensitively depends on polymerization conditions, this might also explain the quantitative disagreements found in the literature regarding microtubule rigidity (Table 2). Kikumoto et al.[55] used an active method evaluating buckling under forces directed inward and found a considerably lower bending rigidity than

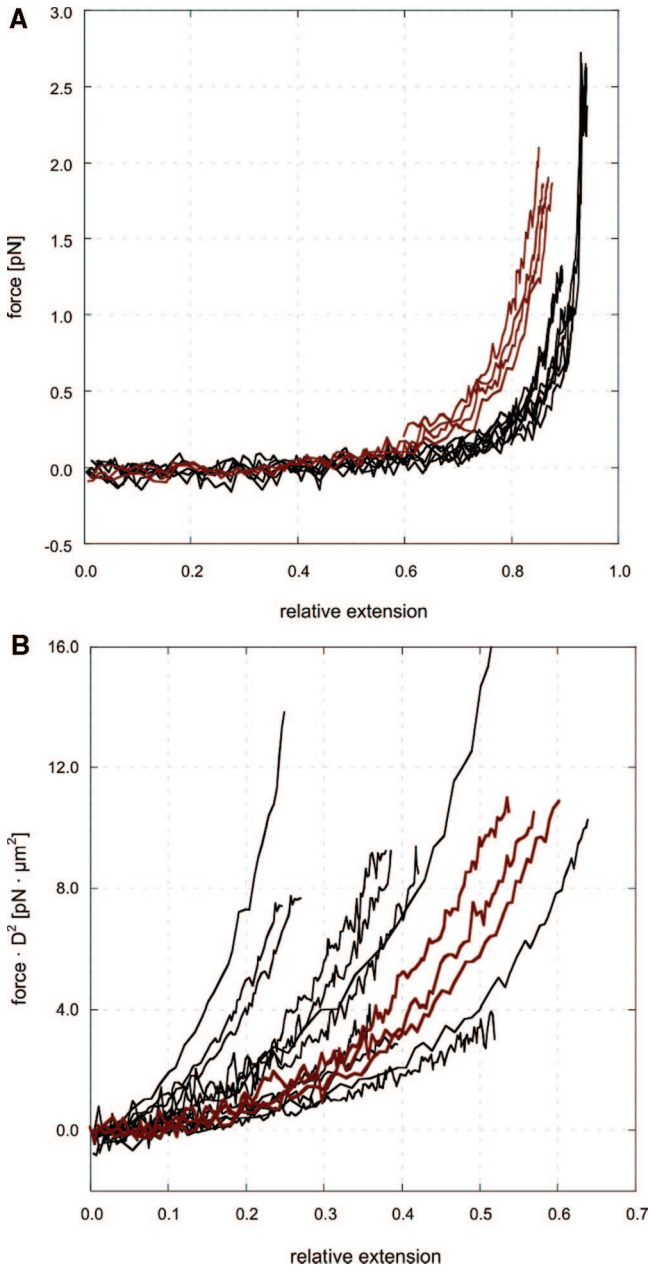

Figure 5. Force-extension measurements of bead-filament-bead constructs. Data is shown for seven actin constructs (A) and eight microtubule constructs (B), some of which were analyzed repeatedly as a control for potential chemical or mechanical degradations over time. The relative extension signal (X) on the horizontal axis is the total extension ξ scaled by the diameter of the beads. Piecewise averaging of the data and averaging over forward and backward traces of one, two, or three successive extensions was performed to reduce the intrinsic noise in the force signal due to Brownian motion of the beads. The notably steeper curves in (A) (red) were measured from a single actin construct. Panel (B) shows microtubule data multiplied by the appropriate bead diameter squared, to allow comparison of data sets obtained with different bead diameters (see eq 3). Curves recorded in succession from one microtubule construct are colored red.

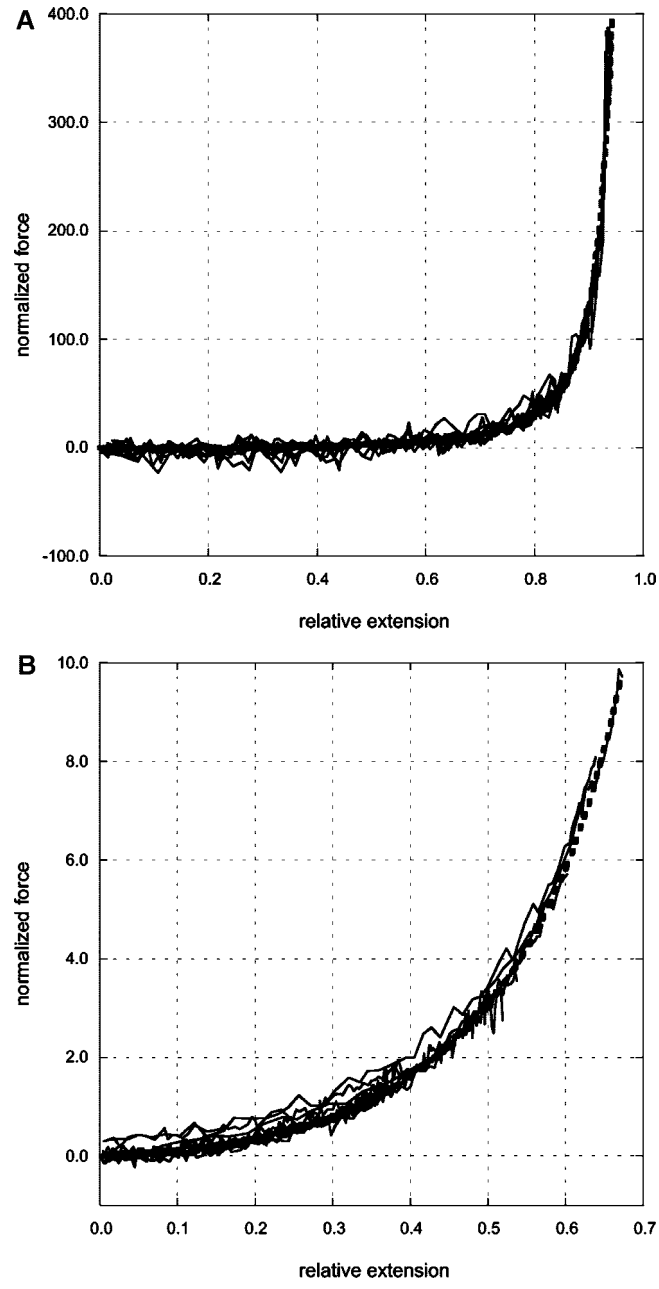

Figure 6. Data from Figure 5 normalized by the individual EI values obtained from fits to the data in Figure 5 plotted as normalized force (normalized force = FD^2/EI) against relative extension. Both for actin (A) and microtubules (B) the curves collapse onto the model curve.

TABLE 1: Elastic Parameters of F-Actin, Literature Values

group	method	EI (10^{-26}N m^2)	L_p (μm)
This paper	active	7.1 ± 0.8	17 ± 2
Dupuis et al.[15]	active	1.5 ± 0.4	3.6 ± 0.1
Riveline et al.[57]	thermal	3.0 ± 0.1	7.4 ± 0.2
Liu and Pollack[58]	active	3.6	8.8
Arai et al.[17]	active	5.5 ± 0.2	13.4 ± 0.5
Ott et al.[20]	thermal	6.9 ± 0.1	16.7 ± 0.2
Gittes et al.[19]	thermal	7.3 ± 0.4	17.7 ± 1.1
Brangwynne et al.[59]	thermal		17.8 ± 2.0

most other reports. Low values were also found in an indirect method modeling the path taken by microtubules propelled by surface-attached kinesin motors.[56] Last but not least, a length dependent bending rigidity of microtubules,[25] if it actually exists, could possibly explain the spread in the results. An argument against that is that our model, assuming a length-independent bending rigidity, fits the shape of the curves very well. The increasing localization of the curvature in the filaments with increasing force should have led to a measurable effect.

Apart from obtaining values for the flexural rigidity of the protein filaments studied, the mechanical model described here can also be utilized for the quantitative analysis of so-called three-bead motor protein experiments. In these experiments, the

TABLE 2: Elastic Parameters of Microtubules, Literature Values

group	method	EI (10^{-24}N m^2)	L_p (mm)
This paper	active	6.1 ± 1.3	1.4 ± 0.3
Felgner et al.[14]	active	1.9 ± 0.1	0.46 ± 0.02
Allersma[60]	active	4.3 ± 1.7	1.0 ± 0.4
Venier et al.[12]	thermal	4.9 ± 0.4	1.2 ± 0.1
Gittes et al.[19]	thermal	22 ± 1	5.2 ± 0.2
Mickey and Howard[22]	thermal	26 ± 2	6.3 ± 0.5
Dogterom and Yurke[23]	thermal	34 ± 7	8.3 ± 1.7
Brangwynne et al.[59]	thermal		1.5−2.8
Kikumoto et al.[55]	active	2.0(+paclitaxel) 7.9 (-paclitaxel)	
Janson and Dogterom[24]	thermal		4.2 ± 0.3 fast growth 6.6 ± 0.9 slow growth
van den Heuvel et al.[56]	thermal		0.24 ± 0.03 at ends

bead displacements induced by the motor protein pulling on the filament are attenuated by the various compliances in the construct. Veigel et al.[30] have interpreted three-bead assay experiments in terms of coupled springs of different stiffnesses. The effective stiffness of the bead-filament attachment is influenced to a large extent by the lateral attachment of the beads. Dupuis et al.[15] have treated this in an approximative manner. With the present model, this stiffness can be calculated quantitatively for different bead sizes and pretensions as the derivative dF/dX of the force-extension curves. Figure 7 shows this stiffness as a function of pretension of both microtubule and actin constructs for different bead sizes obtained by differentiating the numerically obtained solutions to eq 2 (see Figure 3B) and using the experimentally found values for the flexural rigidiy. Couterintuitively, at relatively low tension in the filament, the effective compliance with microtubules is comparable to that achieved with actin filaments, although the bending stiffness of actin is about 100× lower than that of microtubules.

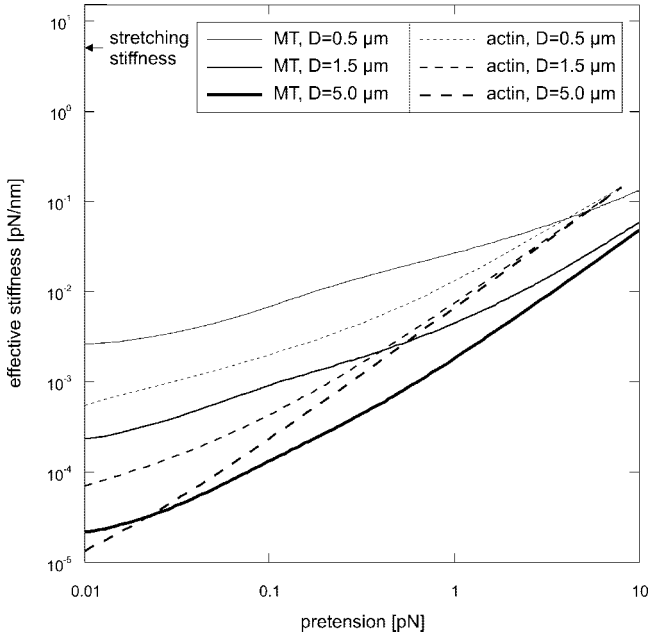

Figure 7. Effective stiffness of the bead-filament-bead construct as a function of the pretension. The experimentally found flexural rigidities found for microtubules (solid lines) and actin filaments (dashed lines) and the indicated values for the bead diameter were used to calculate the stiffness of the bead-filament-bead constructs. The arrow points to the stretching stiffness of the filaments that would be reached asymptotically at high forces.

Conclusions

We have presented an experimental study of the flexural rigidity of actin filaments and microtubules. The force-extension data are interpreted with a numerical model, which distinguishes three force regimes. Analytical solutions have been derived for each of the three regimes. We fitted the experimental data to an interpolation formula for the intermediate and high-force regimes, yielding for the flexural rigidity of actin filaments $EI = (7.1 \pm 0.8) \times 10^{-26}$ nm^2 (persistence length $L_p = 17.2$ μm) and for microtubules $EI = (6.1 \pm 1.3) \times 10^{-24}$ nm^2 ($L_p = 1.4$ mm). Using our results and our model, we predict the stiffness of bead-filament-bead constructs as a function of pretension, which is important for three-bead molecular motor assays. We expect that the experimental geometry we present here and the model to interpret the result will provide a useful method to study details of the elastic response of semiflexible biopolymers.

Acknowledgment. We thank Iwan Schaap, Mikhail Korneev, and Pedro de Pablo for purifying tubulin, and Jeroen van Zon, Bram van den Broek, and Erwin Peterman for fruitful discussions. This work is part of the research program of the Stichting voor Fundamenteel Onderzoek der Materie (FOM), which is financially supported by the Nederlandse Organisatie voor Wetenschappelijk Onderzoek (NWO). C.F.S was further supported by the Center for the Molecular Biology of the Brain (CMPB), funded by the Deutsche Forschungsgemeinschaft (DFG).

Supporting Information Available: Detailed derivation of the model and a derivation of the approximate formula. A figure illustrates the geometry and the variables. This material is available free of charge via the Internet at http://pubs.acs.org.

References and Notes

(1) de Gennes, P.-G. *Scaling Concepts in Polymer Physics*; Cornell University Press: Ithaca, NY, 1979.
(2) de Gennes, P. G. *Phys. Lett. A* **1972**, *38*, 339–340.
(3) Landau, L. D.; Lifshitz, E. M.; Pitaevskii, L. P. *Statistical Physics*; Pergamon Press: Oxford, NY, 1980.
(4) Howard, J. *Mechanics of motor proteins and the cytoskeleton*; Sinauer Associates: Sunderland, MA, 2001.
(5) Alberts, B.; Johnson, A.; Lewis, J.; Raff, M.; Roberts, K.; Walter, P. *Molecular Biology of the Cell*, 5th ed.; Garland Publishing, Inc.: New York, 2008.
(6) Gittes, F.; Schnurr, B.; Olmsted, P. D.; MacKintosh, F. C.; Schmidt, C. F. *Phys. Rev. Lett.* **1997**, *79*, 3286–3289.
(7) Schnurr, B.; Gittes, F.; MacKintosh, F. C.; Schmidt, C. F. *Macromolecules* **1997**, *30*, 7781–7792.
(8) MacKintosh, F. C.; Schmidt, C. F. *Curr. Opin. Colloid Interface Sci.* **1999**, *4*, 300–307.
(9) Koenderink, G. H.; Atakhorrami, M.; MacKintosh, F. C.; Schmidt, C. F. *Phys. Rev. Lett.* **2006**, *96*, 138307.
(10) Gittes, F.; MacKintosh, F. C. *Phys. Rev. E* **1998**, *58*, R1241−R1244.
(11) Morse, D. C. *Phys. Rev. E* **1998**, *58*, R1237−R1240.
(12) Venier, P.; Maggs, A. C.; Carlier, M. F.; Pantaloni, D. *J. Biol. Chem.* **1994**, *269*, 13353–13360.
(13) Elbaum, M.; Fygenson, D. K.; Libchaber, A. *Phys. Rev. Lett.* **1996**, *76*, 4078–4081.
(14) Felgner, H.; Frank, R.; Schliwa, M. *J. Cell Sci.* **1996**, *109*, 509–516.
(15) Dupuis, D. E.; Guilford, W. H.; Wu, J.; Warshaw, D. M. *J. Muscle Res. Cell Motil.* **1997**, *18*, 17–30.
(16) Fygenson, D. K.; Elbaum, M.; Shraiman, B.; Libchaber, A. *Phys. Rev. E* **1997**, *55*, 850–859.
(17) Arai, Y.; Yasuda, R.; Akashi, K.; Harada, Y.; Miyata, H.; Kinosita, K.; Itoh, H. *Nature* **1999**, *399*, 446–448.

(18) Takasone, T.; Juodkazis, S.; Kawagishi, Y.; Yamaguchi, A.; Matsuo, S.; Sakakibara, H.; Nakayama, H.; Misawa, H. *Jpn. J. Appl. Phys* **2002**, *41*, 3015–3019.
(19) Gittes, F.; Mickey, B.; Nettleton, J.; Howard, J. *J. Cell Biol.* **1993**, *120*, 923–934.
(20) Ott, A.; Magnasco, M.; Simon, A.; Libchaber, A. *Phys. Rev. E* **1993**, *48*, R1642−R1645.
(21) Isambert, H.; Venier, P.; Maggs, A. C.; Fattoum, A.; Kassab, R.; Pantaloni, D.; Carlier, M. F. *J. Biol. Chem.* **1995**, *270*, 11437–44.
(22) Mickey, B.; Howard, J. *J. Cell Biol.* **1995**, *130*, 909–917.
(23) Dogterom, M.; Yurke, B. *Science* **1997**, *278*, 856–860.
(24) Janson, M. E.; Dogterom, M. *Biophys. J.* **2004**, *87*, 2723–2736.
(25) Pampaloni, F.; Lattanzi, G.; Jonas, A.; Surrey, T.; Frey, E.; Florin, E. L. *Proc. Natl. Acad. Sci. U.S.A.* **2006**, *103*, 10248–10253.
(26) de Pablo, P. J.; Schaap, I. A. T.; MacKintosh, F. C.; Schmidt, C. F. *Phys. Rev. Lett.* **2003**, *91*, 098101.
(27) Schaap, I. A. T.; Carrasco, C.; de Pablo, P. J.; MacKintosh, F. C.; Schmidt, C. F. *Biophys. J.* **2006**, *91*, 1521–1531.
(28) Schaap, I. A. T.; Hoffmann, B.; Carrasco, C.; Merkel, R.; Schmidt, C. F. *J. Struct. Biol.* **2007**, *158*, 282–292.
(29) Finer, J. T.; Simmons, R. M.; Spudich, J. A. *Nature* **1994**, *368*, 113–119.
(30) Veigel, C.; Bartoo, M. L.; White, D. C. S.; Sparrow, J. C.; Molloy, J. E. *Biophys. J.* **1998**, *75*, 1424–1438.
(31) deCastro, M. J.; Fondecave, R. M.; Clarke, L. A.; Schmidt, C. F.; Stewart, R. J. *Nat. Cell Biol.* **2000**, *2*, 724–729.
(32) Allersma, M. W.; Gittes, F.; deCastro, M. J.; Stewart, R. J.; Schmidt, C. F. *Biophys. J.* **1998**, *74*, 1074–85.
(33) Peterman, E. J. G.; Gittes, F.; Schmidt, C. F. *Biophys. J.* **2003**, *84*, 1308–1316.
(34) Atakhorrami, M.; Sulkowska, J. I.; Addas, K. M.; Koenderink, G. H.; Tang, J. X.; Levine, A. J.; MacKintosh, F. C.; Schmidt, C. F. *Phys. Rev. E* **2006**, *73*, 061501.
(35) Atakhorrami, M.; Addas, K. M.; Schmidt, C. F. *Rev. Sci. Instrum.* **2008**, *79*, 043103.
(36) Gittes, F.; Schmidt, C. F. *Eur. Biophys. J. Biophys. Lett.* **1998**, *27*, 75–81.
(37) Gittes, F.; Schmidt, C. F. *Methods Cell Biol.* **1998**, *55*, 129–156.
(38) WilliamsJr., R. C.; Lee, J. C. In *Structural and Contractile Proteins (Part B: The Contractile Apparatus and the Cytoskeleton)*; Frederiksen, D. W., Cunningham, L. W., Eds.; Academic Press, Inc.: San Diego, CA, 1982; Vol. 85, pp 376−385.
(39) Pardee, J. D.; Spudich, J. A. In *Structural and Contractile Proteins (Part B: The Contractile Apparatus and the Cytoskeleton)*; Frederiksen, D. W., Cunningham, L. W., Eds.; Academic Press, Inc.: San Diego, CA, 1982; Vol. 85, pp 164−181.
(40) Ishijima, A.; Kojima, H.; Funatsu, T.; Tokunaga, M.; Higuchi, H.; Tanaka, H.; Yanagida, T. *Cell* **1998**, *92*, 161–171.
(41) Kron, S. J.; Toyoshima, Y. Y.; Uyeda, T. Q.; Spudich, J. A. *Methods Enzymol.* **1991**, *196*, 399–416.
(42) Svoboda, K.; Schmidt, C. F.; Schnapp, B. J.; Block, S. M. *Nature* **1993**, *365*, 721–727.
(43) Svoboda, K.; Block, S. M. *Annu. Rev. Biophys. Biomol. Struct.* **1994**, *23*, 247–85.
(44) Peterman, E. J. G.; van Dijk, M. A.; Kapitein, L. C.; Schmidt, C. F. *Rev. Sci. Instrum.* **2003**, *74*, 3246–3249.
(45) Berg-Sørensen, K.; Peterman, E. J. G.; Weber, T.; Schmidt, C. F.; Flyvbjerg, H. *Rev. Sci. Instrum.* **2006**, *77*, 063106.
(46) Feynman, R. P. *The Feynman lectures on physics*; Addsion Wesley: Redwood City, CA, 1989; Vol. 2.
(47) Gittes, F.; Schmidt, C. F. *Opt. Lett.* **1998**, *23*, 7–9.
(48) Wong, J.; Chilkoti, A.; Moy, V. T. *Biomol. Eng.* **1999**, *16*, 45–55.
(49) Gittes, F.; Mickey, B.; Nettleton, J.; Howard, J. *J. Cell Biol.* **1993**, *120*, 923–934.
(50) Kojima, H.; Ishijima, A.; Yanagida, T. *Proc. Natl. Acad. Sci. U.S.A.* **1994**, *91*, 12962–12966.
(51) Higuchi, H.; Yanagida, T.; Goldman, Y. E. *Biophys. J.* **1995**, *69*, 1000–1010.
(52) Bustamante, C.; Marko, J. F.; Siggia, E. D.; Smith, S. *Science* **1994**, *265*, 1599–1600.
(53) Chretien, D.; Metoz, F.; Verde, F.; Karsenti, E.; Wade, R. H. *J. Cell Biol.* **1992**, *117*, 1031–1040.
(54) Díaz, J. F.; Valpuesta, J. M.; Chacon, P.; Diakun, G.; Andreu, J. M. *J. Biol. Chem.* **1998**, *273*, 33803–33810.
(55) Kikumoto, M. *Biophys. J.* **2006**, *90*, 1687–1696.
(56) van den Heuvel, M. G. L.; Bolhuis, S.; Dekker, C. *Nano Lett.* **2007**, *7*, 3138–3144.
(57) Riveline, D.; Wiggins, C. H.; Goldstein, R. E.; Ott, A. *Phys. Rev. E* **1997**, *56*, R1330−R1333.
(58) Liu, X. M.; Pollack, G. H. *Biophys. J.* **2002**, *83*, 2705–2715.
(59) Brangwynne, C. P. *Biophys. J.* **2007**, *93*, 346–359.
(60) Allersma, M. W. Ph.D. Thesis, University of Michigan, Ann Arbor, MI, 2000.

JP808328A